Modeling dental implant insertion

A. Dorogoy, D. Rittel(*) , K. Shemtov-Yona , and R. Korabi

Faculty of Mechanical Engineering

Technion

32000, Haifa, Israel

ABSTRACT

The success of dental implantation is connected to the so-called implant primary stability, a synonym for very small implant motions inside the bone. The primary stability is related to the applied peak torque to the implant during the insertion process. This work simulates the process of insertion of a typical commercial implant into the mandible bone using a 3D dynamic non-linear finite-elements software. The model considers the geometrical and mechanical properties of the implant, the bone-implant friction, and the insertion procedure parameters, namely angular velocity and normal load. The numerical results assess the influence of those parameters on the insertion torque and the bone damage. It is found that, within the model's assumptions, the angular velocity up to 120 rpm has little or no effect on the process. The normal load enforces an extrusion process in addition to the screwing one. The respective contribution of the cortical and trabecular bone components to the insertion torque reveals that, despite its significantly lower strength, the trabecular bone has a definite contribution to the insertion process. This work shows that if the various physical, geometrical and mechanical parameters of the bone-implant system are well-defined, the insertion process can be simulated prior to the surgical act, and predict, tailor and maximize the success of dental implantation in a personalized manner.

Keywords: Dental Implants, Primary Stability, Numerical Model, Insertion Torque, Bone Damage.

* Corresponding author: merittel@technion.ac.il; Tel.: +972-4-8293131

1. Introduction

Successful osseointegration is a degree of implant stability which occurs after implant integration. This end result is related to two terms, namely primary and secondary implant stability. Primary stability characterizes the *mechanical* engagement of the implant right after its insertion (Orenstein et al., 2000)(Javed and Romanos, 2010), while secondary stability is the result of (longer term) bone regeneration and remodeling (*biological* process) around the inserted implant (Meredith, 2008). Primary and secondary stability are closely related, as poor primary stability is one of the major causes of implant failure (Javed and Romanos, 2010). Implant micro-movements exceeding the range of 50 to 150 μm can harm or even break freshly created biological bonds between the growing bone and the implant, before final osseointegration is achieved (Szmukler-Moncler and Salama, 1998) (Szmukler-Moncler et al., 2000) (Kawahara et al., 2003).

In addition, immediate loading of dental implants, i.e. functional loading (with occlusal contacts) immediately after implantation, is the main agreed-upon option for the rehabilitation of missing teeth. Several studies (Javed et al., 2013)(Schwartz-Dabney and Dechow, 2002) have reported high success rates with immediate loading of dental implants, which are attributed to high primary stability. A recommended maximum insertion torque value of at least 40 Ncmcm or mm? needs to be reached during implants insertion in order to undergo immediate loading protocol (Degidi and Piattelli, 2005)(Javed and Romanos, 2010)(Goswami et al., 2015).

Several factors affect the implant primary stability. Among those are the bone type, bone quantity and quality, implant geometry, and surgical technique (Romanos, 2009)(Atsumi et al., 2007). Several methods exist in order to assess the implant primary stability. Among them are insertion torque measurement (Alsaadi et al., 2007) and the resonant frequency analysis (RFA) (Schulte and Lukas, 1992)(Meredith et al., 1996). These methods are limited by the fact that they are *postoperative*, and thus do not permit optimization of implant insertion with sufficient primary stability (Atsumi et al., 2007).

Quantification of implant stability *prior to* insertion during the treatment planning phase, may provide significant information as to the individualized "optimal healing" time and personalized "treatment protocol".

The finite element method (FEM) is a widely used stress analysis method for the investigation of the biomechanical behavior of bone-implant-rehabilitation components, and simulation/evaluation of their mechanical interaction, which is otherwise extremely difficult to investigate experimentally, either in vitro or in vivo. The FEM enables researchers to apply different loadings configurations and determine the displacement and the stress levels experienced by the tooth, prosthesis, implant, and bone (Pesqueira et al., 2014).

Several studies have used the FE models to simulate and study dental implant insertion and the specific issue of primary stability. Olsen et al. (Olsen et al., 2005) calculated the axial stability of the dental implant. Their model is quite simplistic, and the reported correlation with experimental results was weak. The model considered cylindrical implants and did not include bone damage during insertion. The work of Bardyn et al. (Bardyn et al., 2010) elaborated on the work of Olsen et al. (Olsen et al., 2005) by using a 3-dimensional (3D) FE solver. The purpose of that study was the prediction of the removal torque of an implant. In that work, the insertion process was not modeled and bone damage occurring during the insertion process was not considered. The implant was placed in its final position and the problem was reduced to the simulation of radial press-fit in which the removal torque is approximated by multiplying the friction coefficient by the total of the radial reaction forces due to press-fit deformation at the thread-bone interface.

A similar approach was used by van Staden et al. (van Staden et al., 2008), in which the finite element method was used to simulate the insertion process of a dental implant into a section of the human mandible. The purpose was to replicate and evaluate the stress profile created within the mandible during the implantation process. Instead of simulating a continuous process, a series of finite element models were constructed and simulated. Each model differed from the preceding one by the fact that the implant was inserted 1mm deeper into the jawbone. The stepwise assumption, together with the assumption of a parallel-threaded implant that does not rotate during insertion into the jawbone, are significant simplifications. Here too, bone

damage during insertion was not considered although the existence of an area of blood and bone interface was assumed between the implant teeth and bone. This interface was found to drastically alter the stress profile within the jawbone. Pre-defined torque levels were assumed for each step, overlooking the fact that the actual torque should actually result from several parameters of the problem at hand (geometrical and mechanical), rather than being prescribed.

Guan et al. (Guan et al., 2011) expanded the study of van Staden et al. (van Staden et al., 2008) in the sense that these authors investigated the effects of the implant thread on the forming and cutting on the surrounding bone. The implantation process was modelled in a continuous manner. Guan et al. (Guan et al., 2011) assumed that the process of implantation is continuous under the application of a constant torque. Moreover, a constant downward axial velocity was applied to the implant as a boundary condition. A "surface to surface" contact was assumed between the bone and implant. One should note here that the prescription of a constant applied torque, which is higher than the actual resisting torque, is expected to create an angular acceleration which usually causes a variable penetration velocity that increases with time. Yet, in the work of Guan et al. (Guan et al., 2011), the constant applied torque was accompanied by the application of a constant downward penetration velocity of the implant. In that case, the penetration velocity should have been the result of both the applied and the resisting torque, and not pre-assumed. Moreover, this analysis did not consider damage to the contacting surfaces, mostly on the bone side.

Finally, none of the above-mentioned analyses considered the effect of a normal load applied to the implant. Such a load is an inherent component of the bone drilling/implant insertion process, which must be taken into account to create a more physical representation of the problem (Pandey and Panda, 2013; Wang et al., 2014).

From the above literature survey, it appears that a complete model of the implant insertion into the jawbone should account for the bone-implant interface as well as the damage caused to the bone. In addition, consistent boundary conditions should be applied, such as to insure that the insertion torque results in fact from the ensemble of characteristics of the problem rather than being used as a prescribed boundary condition, if one wants to have a realistic model of the process.

In this study, 3D explicit continuous nonlinear FEM analyses are performed. Elastic plastic material models which include failure and damage are assumed for the cortical and cancellous bone, while the implant is considered rigid (as a first approximation). A constant angular velocity is applied to the implant together with a vertical downward force. Likewise, a normal load is applied to the implant. The result of the analysis is an evaluation of the resisting torque of the bone together with the characterization of the bone damage for systematic variations of the model parameters.

2. Material and methods

The process of inserting a randomly selected, yet representative standard commercial implant (MIS SEVEN, Fig 1) into the mandible bone, was simulated numerically using the commercial finite elements package Abaqus Explicit version 6.14-2 (Simulia, 2014a). The model is three dimensional and the analyses are dynamic, continuous and non-linear. The simulation assumed a rigid implant rotating at a constant rotational velocity with an axially applied load downward. The initial insertion hole was 2.8 mm in diameter, which is accordance to MIS protocol (ref WEBSITE). The rotational velocity considered were in the range 30-120 rpm while the vertical load was (arbitrarily) varied in the range of 1-180 N. Note that the commonly applied angular velocities are close to 30 rpm, so that the above-quoted higher values used are used for the sake of computational time reduction only. Consequently, bone heating effects related to the insertion process are not considered in this work, even if they could be quite significant at high insertion speeds (Lee et al., 2012). The dimensions, material models and parameters, mesh properties and boundary conditions are detailed in the sequel.

2.1 Assembly dimensions

The implant is 3.75mm diameter, 13mm length, and it features 5 micro-rings on its neck. It has conical shape and threads that increase in thickness along the implant body, as shown in Fig. 1. The neck height is 3 mm and uppermost ~1 mm has no micro-rings.

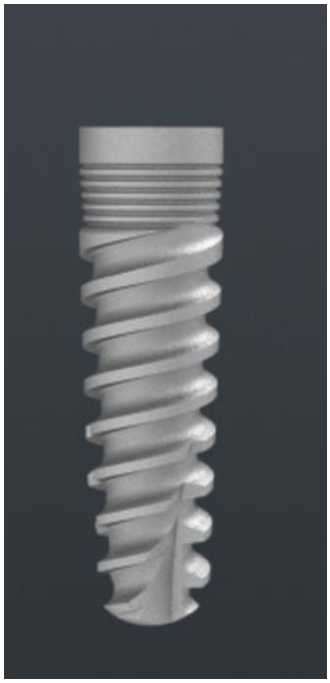

Figure 1: The MIS SEVEN implant: 3.75mm diameter, 13mm length. Reprinted from: http://www.misimplants.com/implants/brands/seven/seven-mf7-13375.html

A typical cross section of the mandible at the facial region was extruded 20 mm along the Z axis. It consists of cortical bone (grey Fig 2) having a thickness of ~2 mm, and of cancellous bone (green in Fig. 2). The overall dimensions are shown in Figs. 2b and 2c. An initial cylindrical cavity having a diameter 2.8 mm and depth of 13.3 mm was created. Since the neck outer diameter of the implant is 3.75 mm, the maximum diametrical misfit is of 0.95 mm between the implant and the pre-processed cavity.

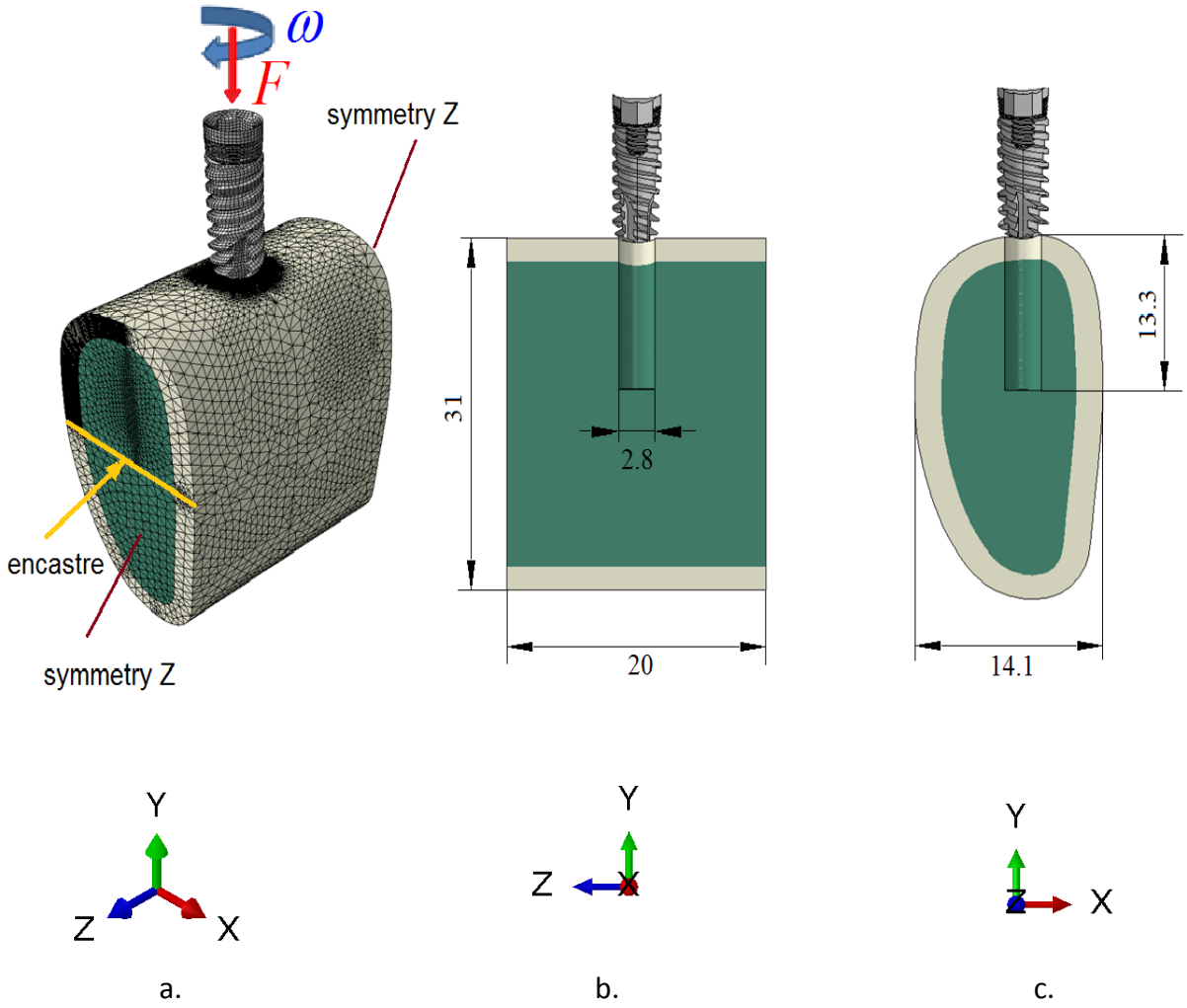

Figure 2: Assembly of the implant and bone and boundary conditions at the beginning of the insertion process. a. Isometric view of the meshed assembly. b. Z-Y cut view. c. X-Y cut view. All dimensions are in mm.

Material properties

The implant was modeled as rigid material having a mass of 0.37 gr. The bone constituents were assumed to be perfectly bonded. The material properties of the bone constituents are detailed in the sequel.

Cortical bone

The cortical bone is known to behave differently in compression and tension (TM and WC, 1992) and was therefore modeled as an elastic-(almost) perfectly plastic material

with Drucker-Prager (DP) representation to account for the above-mentioned asymmetry (Fig. 3). Ductile failure with damage evolution (Simulia, 2014b) was used as a failure criterion. The tensile and compressive yield strengths were taken as 120 and 180 MPa, respectively (Fig. 3). The plastic strain at fracture was set to 1%. in tension and 2% in compression (TM and WC, 1992). This reference should be written correctly. The "damage evolution value", expressing the residual displacement from attainment of the critical strain until final element deletion, was set to zero after verifying the lack of influence of this parameter's value on the calculated IT. Stated otherwise stated, failure of the cortical bone is considered to occur abruptly.

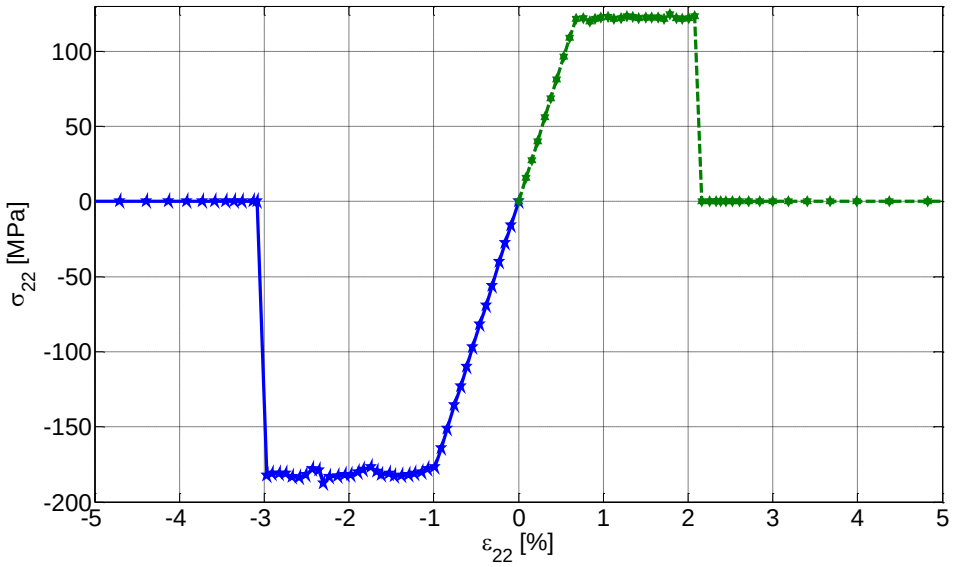

Figure 3: Unidirectional tension and compression of a cortical bone.

Cancellous bone

The cancellous bone is a cellular material (Ashby and Medalist, 1983), and is approximated here by an elastic-(almost ideal) plastic material model. We did not attempt to include in this work the strain hardening phase at large strains, that results from cell densification processes. Although it is significantly weaker than the cortical bone, it was found that the cancellous bone plays an important role in primary stability of implants in the presence or absence of cortical bone (Marquezan et al., 2014). The Young's modulus, Poisson ratio and fracture strain were all taken from

Guan et al. (Guan et al., 2011), while "representative" yield stresses were set to $10 < \sigma_Y < 62$ MPa.

It has been shown experimentally and verified numerically that the maximum compressive stress of cylindrical specimens made of human trabecular bone ranges between 10 and 80 MPa for various bone volume fractions, i.e. the ratio of the bone (cortical or trabecular) volume (BV) over the total bone volume (TV). These stress values correspond to small strains (typically less than 0.1) prior to densification. An empirical formula for the ultimate compressive stress (σ_{uts}) of a bone as a function of the bone volume fraction and the mineral content (ash fraction α) was derived (Hernandez et al., 2001):

$$\sigma_{uts} = 794.33(BV/TV)^{1.92}\alpha^{2.79} \qquad (1)$$

Using an ash fraction of $\alpha = 0.6$, which is common, the predicted stresses of this formula together with the experimental results (Hambli, 2013) are plotted in Fig. 4. The limit values of σ_Y which are used in the numerical analyzes are plotted as well. It can be observed that there is a good agreement between the experimental results (Hambli, 2013) and the formula (Hernandez et al., 2001). Using in the numerical model $\sigma_Y = 62$ MPa corresponds approximately to bone volume fraction of ~54%, while $\sigma_Y = 10$ MPa corresponds to a bone volume fraction of 17%-23%.

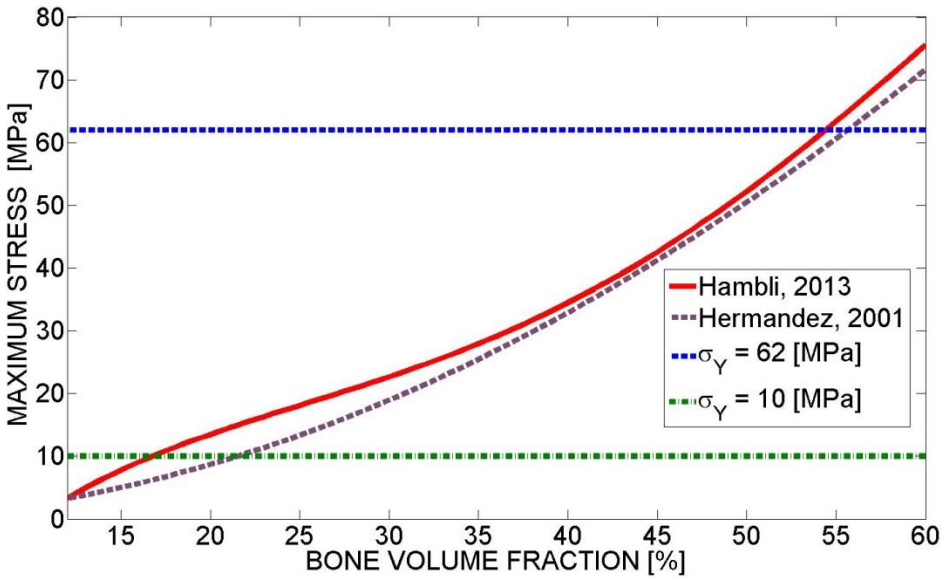

Figure 4: The maximum experimental compressive stresses vs bone volume fraction of (Hambli, 2013) and the formula of (Hernandez et al., 2001) together with the limit values of σ_Y which were considered numerically.

The numerical model stress-strain curves for σ_Y = 62 MPa and σ_Y = 10 MPa which were used for the trabecular elastic-plastic model are shown in Fig. 5 together with the stress-strain curves given by Gibson (Gibson, 1985) for relative density ρ/ρ_s of 0.3, 0.4 and 0.5. The density of the solid bone is denoted ρ_s. It is shown that the compressive strength of the solid trabecular bone can reach 123 MPa. The value 62 MPa is only 50% of the maximum compressive strength.

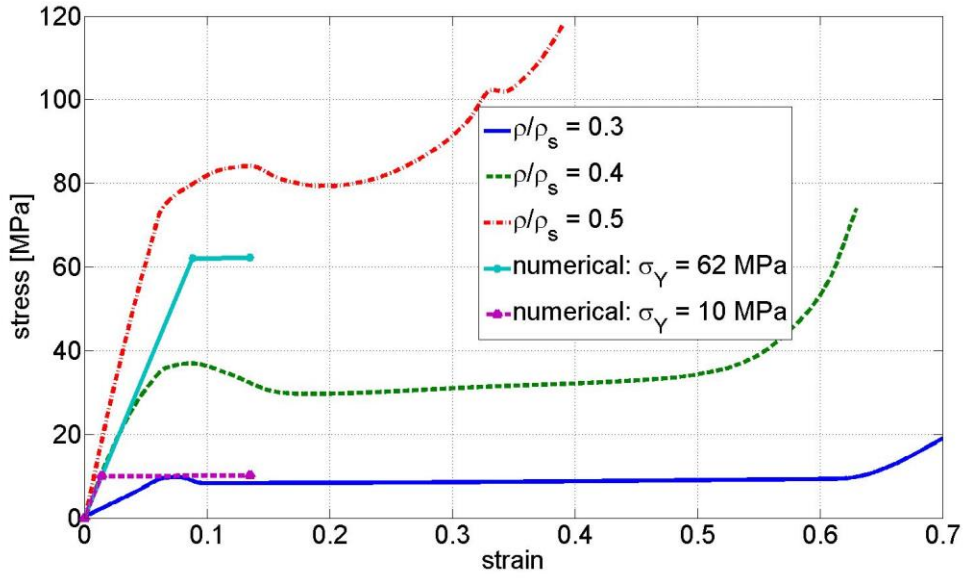

Figure 5: The numerical elastic-plastic model in comparison to stress-strain curves in compression which were obtained by Gibson (Gibson, 1985).

Numerical experimentation with different failure strains together with the elastic-plastic model revealed that the value of the failure strain has a small effect on the torque results hence the value of ε_p^f=0.135 (Guam et al, 2011) was used. The trabecular bone is softer than the cortical bone, hence a small value of 10 μm was given as damage evolution. This value was given just to increase stability of the numerical solution during element deletion and does not affect the torque results.

The typical material properties, based on (Guan et al., 2011; Reilly and Burstein, 1974; TM and WC, 1992; van Staden et al., 2008), were used in the simulations and are summarized in Table 1.

Table 1: Material properties

	ρ [Kg/m^3] density	E [MPa] Young's modulus	ν Poisson ratio	σ_Y [MPa] yield stress	β [^{o}] Drucker Prager	ε_p^T [%] Fracture plastic strain tension	ε_p^C [%] Fracture plastic strain compression	Damage evolution [μm]
Cortical bone	1900	18000	0.35	180	30	1	2	0.0
Cancellous bone	1000	700	0.35	10-62	0	0.135	0.135	10

2.3 Mesh

The implant was meshed with 8051 rigid elements: 7448 linear quadrilateral elements of type R3D4 and 603 linear triangular elements of type R3D3. The meshed implant is shown in Fig. 6a.

The bone was meshed with 858933 linear tetrahedral elements of type C3D4. The mesh of the assembly is shown in Fig. 2a. The region around the cavity was meshed with small elements of size 0.2-0.3 mm, while the cortical bone around the cavity was made even denser, with a seed size of 0.1 mm as shown in Fig 6b.

Numerical convergence was verified in preliminary calculations with different mesh sizes.

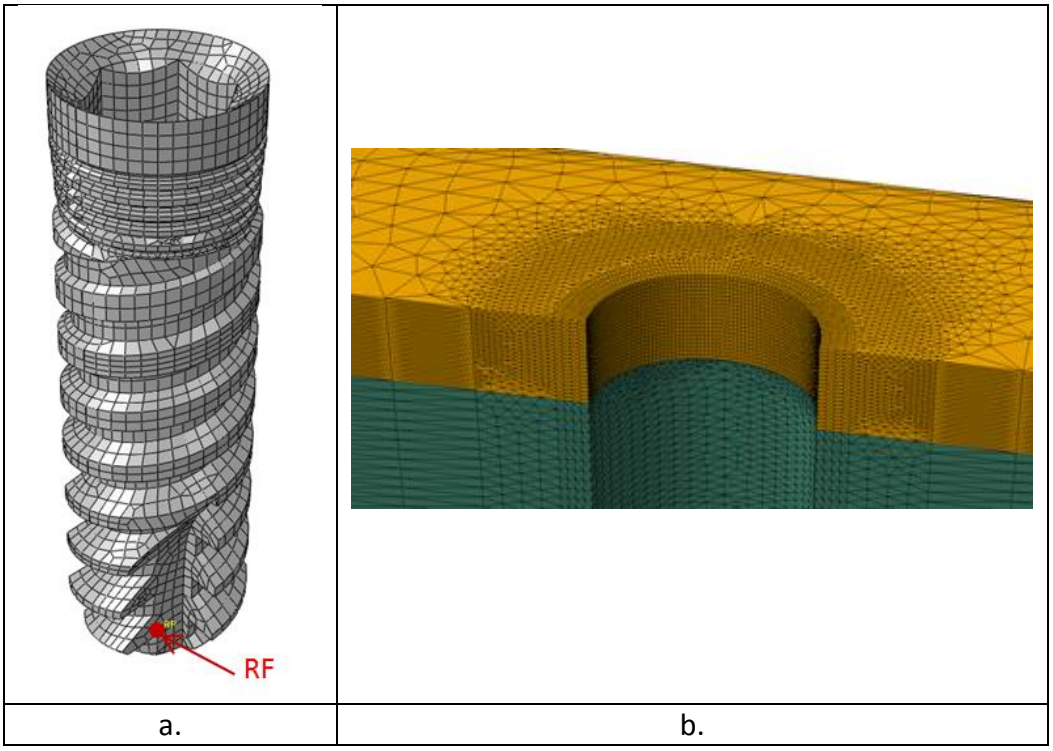

a. b.

Figure 6: a. The meshed implant. b. The mesh of the cortical bone around the hole. RF (reference point) indicates the point of application of vertical load and implant rotations.

2.4 Boundary conditions

Symmetry conditions were applied on both planes of the bone with the normal pointing in the Z direction ($n_z = \pm 1$). A line along on the plane $n_z = \pm 1$ (Fig. 2a) was fixed in all directions to prevent rigid body motions of the assembly.

The rigid implant was only allowed to rotate and move downwards in the y direction. A constant angular velocity (ω_y) in the range 30-120 rpm was applied to the implant on the reference point shown in Fig. 6a. A constant downward force (F), in the range of 1-180 N was applied as well on the rigid implant on the reference point. The angular velocity and vertical load are shown in Fig. 2a.

The general contact algorithm of Abaqus (Simulia, 2014b) was used with element-based surfaces which can adapt to the exposed surfaces of the current non-failed elements. Abaqus' frictional tangential behavior with the penalty formulation was

adopted. A frictional Coulomb contact was used with a constant coefficient of friction 0.61 (Grant et al., 2007; Guan et al., 2011). All the surfaces that may become exposed during the analysis, including faces that are originally in the interior of bone were included in the contact model. We assumed that contact nodes still take part in the contact calculations even after all of the surrounding elements have failed. These nodes act as free-floating point masses that can experience contact with the active contact faces (Simulia, 2014b).

3. Results

Four different topics are addressed here. Firstly, the choice of computational angular velocity is justified. Secondly, the effect of the trabecular yield stress (or bone volume fraction) on the IT is studied. The third topic addresses the respective contribution of each bone component (trabecular and cortical) to the IT. A fixed vertical load of 5N is used in the first three sections. In the fourth section, the vertical load component was systematically varied for a fixed angular velocity, and its influence assessed for a series of process parameters such as IT, number of revolution for full insertion and bone damage.

3.1 Effect of the angular velocity on the insertion torque

The IT was calculated for 4 different angular velocities and 2 different material yield stresses of the trabecular bone: 1. a dense bone having σ_Y = 62 MPa, and 2. a soft bone having σ_Y = 10 MPa. A constant vertical load F = 5 N was applied. The angular velocities which were considered were: ω = 30, 60 and 120 rpm. A typical numerical IT graph for the case of a dense trabecular bone and angular velocity of 30 rpm is presented in Fig. 7a. It can be observed that the numerical results vibrate. These vibrations are partly due to the element deletion procedure. A Butterworth filter was applied to filter the high frequencies. The resulting filtered IT is shown as well. The filtered IT graph preserves the characteristics of the original IT graph in a clearer way hence filtering is used for all following IT results in the sequel. Three distinct regions can be identified, as marked in Figure 7a: Entrance, threads penetration, and neck

penetration. The "entrance" phase is associated with the insertion of the narrow lower part of the implant into the cortical bone that has a thickness of 2 mm. The implant position at the end of the entrance is shown in Fig. 7b. During the "threads penetration" phase, the implant is inserted deep into the trabecular bone. The IT value first drops because of the strength differences between the cortical and trabecular bones, and then increases steadily due to the increased contact areas and frictional forces, together with the enlargement of the cavity in the cortical bone. At the end of this phase, the implant body portion is completely surrounded by bone and the IT reaches its peak value. The position of the implant at the end of the "threads penetration" phase is shown in Fig. 7c. During the last phase – "neck penetration" – the neck of the implant is inserted into the bone.

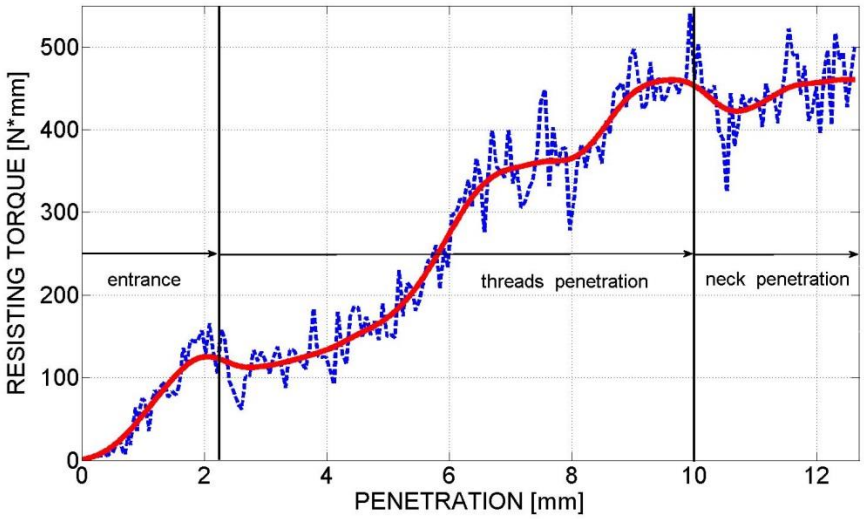

a.

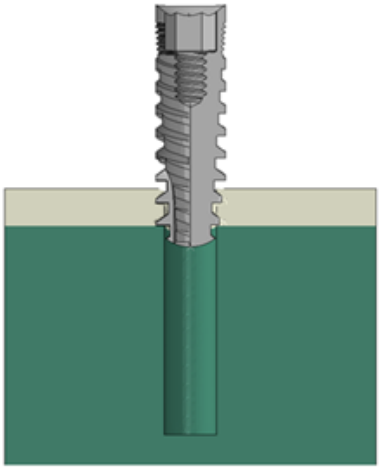

b.

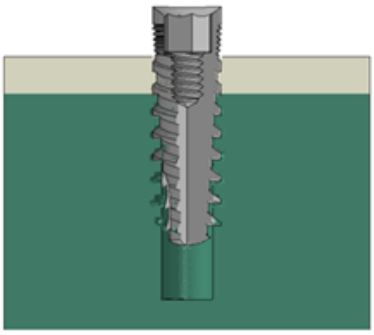

c.

Figure 7: a. The insertion torque for applied vertical forces of 5 N and angular velocities 30rpm with σ_Y = 62 MPa. Note the three distinct regions: Entrance, threads penetration and neck penetration. b. The position of the implant at the beginning of the "threads penetration". c. The position of the implant at the end of the "threads penetration".

10 MPa for angular velocities of 60 rpm and 120 rpm. For σ_Y = 10 MPa the insertion process in both angular velocities results in a very similar IT distribution. It can be concluded that for low yield stresses, the angular velocity has no appreciable effect on the IT. For σ_Y = 62 MPa the insertion process at both angular velocities results in very similar ITs up to the final insertion phase of the neck. Hence a third angular velocity, ω = 30 rpm was tested. It can be observed that during the first two phases of insertion (entrance and threads penetration) the IT results are quite similar and the value of IT at the end of "threads penetration" phase is similar- 450 Nmm. For ω = 30 rpm this is the peak value while for ω = 60 rpm and ω = 120 rpm there is some rise up of the IT during neck insertion which grows with the higher angular velocities. It is concluded that for very high yield stresses, the angular velocity does not have a significant effect up to end of the threads penetration, but might have some small effect during the last phase of neck penetration, as a result of the insertion dynamics. The solution with ω = 30 rpm clearly shows that the peak IT is reached at the end of the "threads penetration" phase.

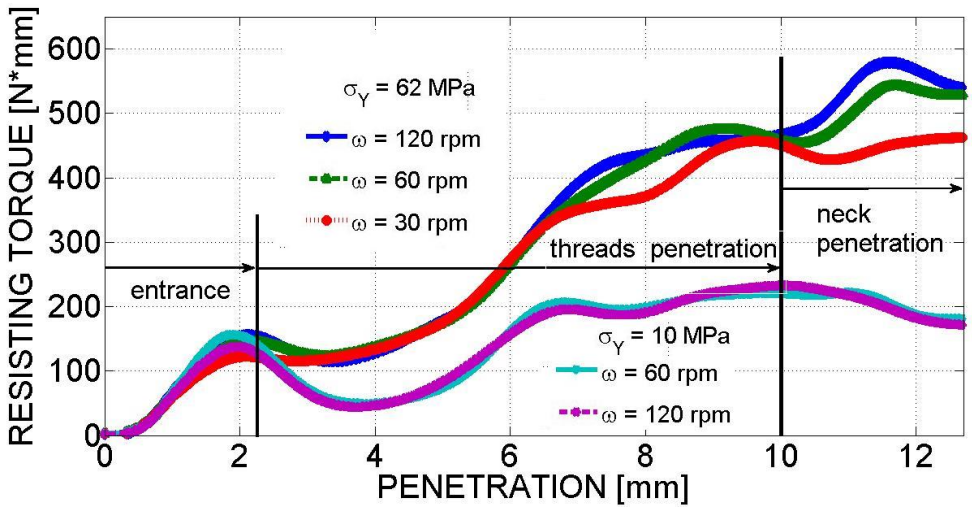

Figure 8: Effect of angular velocity on the IT for two value of σ_Y (trabecular): 10 and 62 MPa.

3.2 Effect of the trabecular bone yield stress on the insertion torque

The IT was calculated for three more values of trabecular yield stresses: σy = 20, 32 and 47 MPa. The same vertical load of 5 N was applied and a fixed angular velocity of ω = 120 rpm was used. The IT evolutions for σ_y = 10, 20, 32, 47 and 62 MPa are shown in Fig. 9a. The three insertion phases are identical for all yield stresses. For all yield stresses the peak value of the IT is reached at the end of the "threads penetration" phase at 10 mm depth. For lower yield stresses of 10 and 20 MPa, there is a small drop in the IT during the last phase of "neck penetration". This drop is due to destruction of the threads on the cortical bone during the neck penetration and inability of the cortical bone to carry torque. This will be further addressed in the next section.

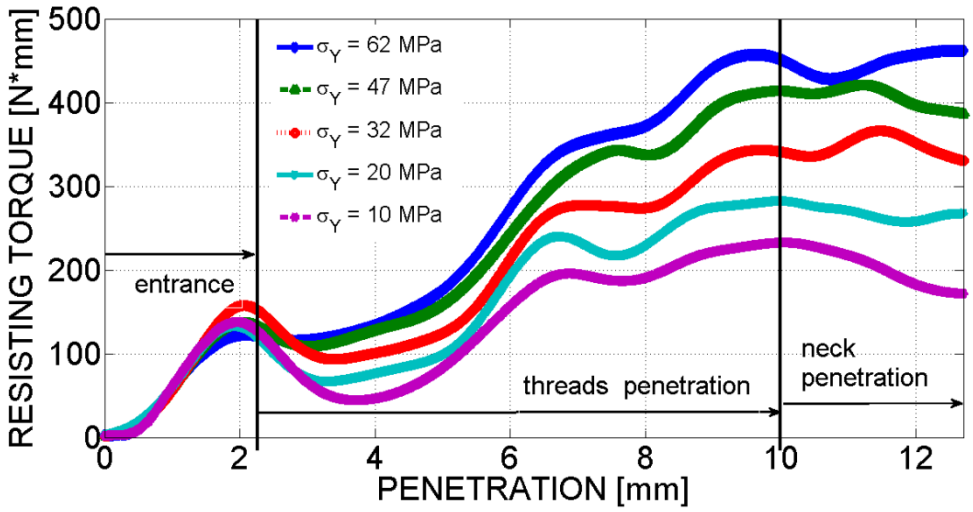

a.

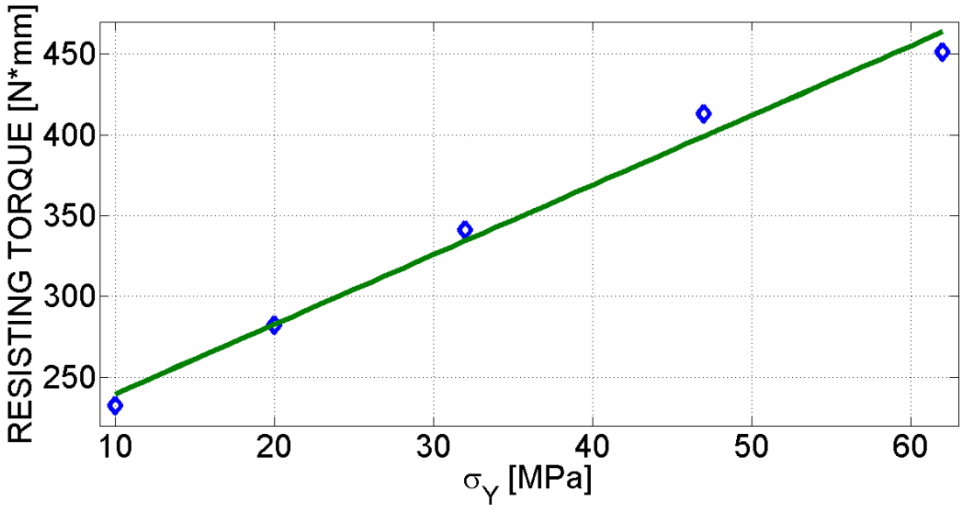

b.

Figure 9: Effect of trabecular bone yield stress on the IT. a. IT of σ_y(trabecular) = 10, 20, 32, 47 and 62 MPa. b. Peak values of IT at the end of the "threads insertion" phase.

The peak values of IT at the end of the "threads penetration" phase are shown in Fig. 9b as a function of the yield stresses. These peak values can be approximated by a linear function. This figure can be used to estimate the expected primary stability using this specific implant for pre-determined personal bone characteristics. If for example, the bone volume fraction of a specific patient is known, Fig. 4 could be used to estimate the yield stress for the numerical model, while Fig, 9b can be used to estimate the achievable peak torque value. Assuming that a peak value of 350 Nmm is needed for primary stability, those results indicate that the patient should have bone volume fraction that corresponds to yield stresses higher than 35 MPa.

3.3 Insertion torque partition between the trabecular and cortical bone

In order to characterize the torque partition between the cortical and trabecular bone, the case of F = 5 N and ω = 120 rpm was solved again, but the strength of the trabecular bone was reduced to 0.1% of its original values. Therefore, the cortical bone is the only mechanically active bone component. Fig. 10a shows the IT vs. depth of penetration for the cortical bone only. It shows it in comparison to the IT variation

already shown in Fig. 9a for the cases of σ_Y = 10 MPa (case 1) and σ_Y = 62 MPa (case 2). Naturally, the entrance phase which involves only the cortical bone is identical for the three examined cases. The slight differences that occur at the entrance phase are due to the filtering process. Until completion of the "thread penetration" phase, the torque grows steadily until it reaches its peak value. Each bone component makes its own distinct contribution to the resultant IT, and that of the trabecular bone is important, a fact that can be justified in terms of its overall contact surface area in spite of its lower strength. Upon completion of the insertion during the "neck penetration" phase, one can notice that the cortical bone's contribution drops rapidly to zero.

The ratio (%) of the IT of the cortical bone alone for cases 1 and 2 is shown in Fig. 10b. The ratio should have been 100% during the entrance phase but because of numerical fluctuations and the filtering process it is close to 100%. In the beginning of the "threads penetration" phase, at a penetration depth of 4 mm, it drops to 70% for case 1 and 25% for case 2. At the end of the threads penetration phase where the IT reaches its peak value the cortical bone carries 73% of the torque for case 1 and 39% for case 2. During the "neck penetration" phase the cortical bone loses its ability to sustain torque and the ratio drops to zero.

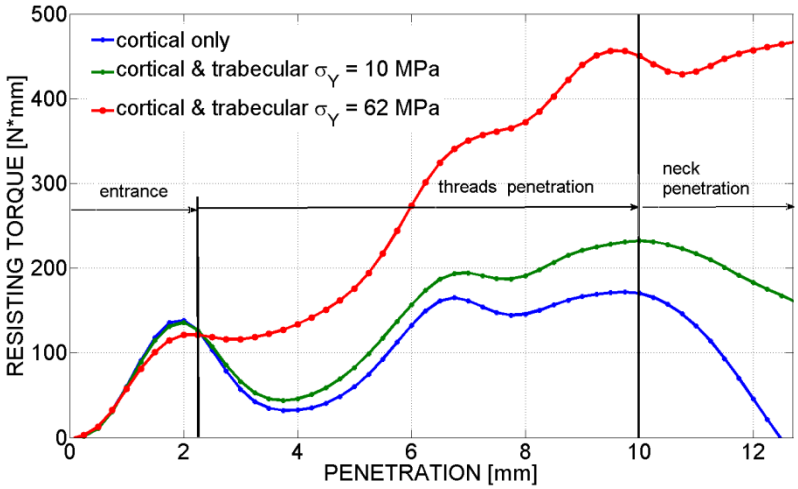

a.

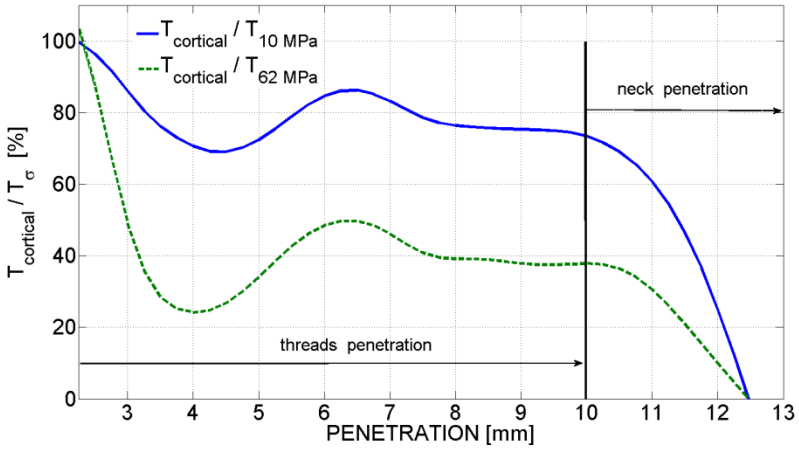

b.

Figure 10: a. The insertion torque for F = 5 N and ω = 120 rpm for cortical bone alone in comparison to a full bone which consist of cortical and trabecular bone having σ_Y = 10 and 62 MPa, respectively. b. The ratio between the torque carried by the cortical bone to the "full torque" carried by both the cortical and trabecular bones having σ_Y = 10 and 62 MPa.

The reason for the inability of the cortical to sustain torque at the end of the insertion process is explained by means of Figs. 11 a-d. Figs. 11 a-b show the cortical bone at the beginning of the "neck penetration" phase while Figs. 12c-d show the cortical bone at the end of the "neck penetration" phase. The trabecular bone (green) can be ignored because of its negligible strength. Figs. 11a and 11c show the location of the implant in relation to the cortical bone at the beginning and end of the "neck penetration" phase respectively. The threads are initially visible in the cortical bone, and are encircled in the cut view (Fig. 11b). However, at the end, they are no longer discernable as shown in the encircled region of the cut view (Fig. 11d). The disappearance of the threads is due to the destruction of the threads during the penetration of the neck with its micro-grooves.

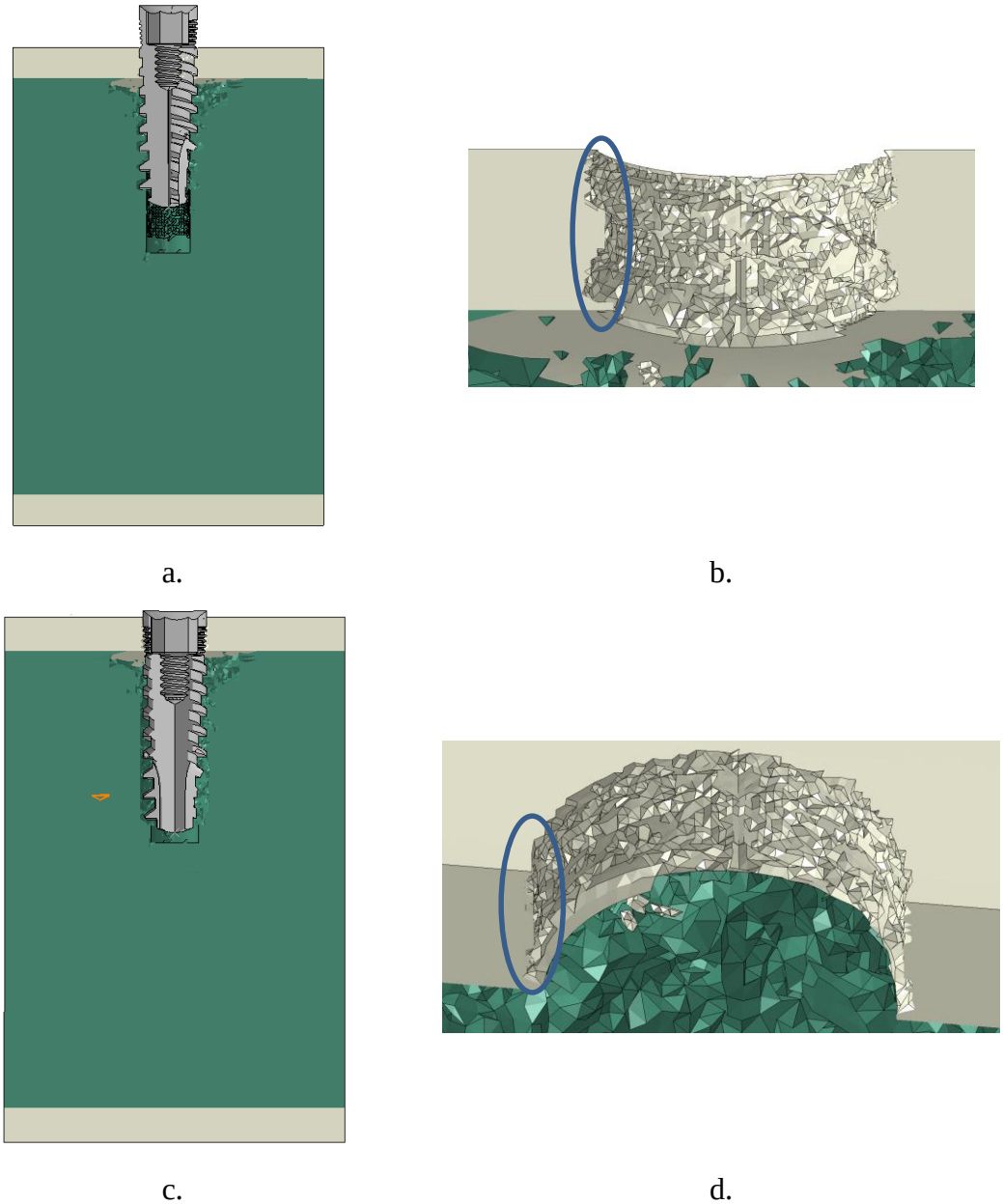

a. b.

c. d.

Figure 11: The damaged cortical bone for F = 5 N and ω = 120 rpm. a. A cut view showing the position of the implant at the beginning of the "neck penetration" phase. b. The cortical bone at the beginning of the "neck penetration" phase. c. A cut view showing the position of the implant at the end of the "neck penetration" phase. d. The cortical bone at the end of the "neck penetration" phase.

3.4 Effect of the applied vertical load

The IT was calculated for applied load levels in the range : 1 N < F < 180 N and implant angular velocity of 120 rpm. This was done for two types of trabecular bone σ_Y = 10 (case 1) and σ_Y =62 MPa (case 2).

3.4.1 Effect on insertion torque

The IT for a bone with σ_Y = 62 MPa, for F = 5, 30, 60, 90, 120, 150 and 180 N are shown in Fig. 11a. Note that for F = 1 N, there was no penetration since the vertical load is not sufficient to cause insertion, and the implant just slowly grinds the cortical bone. This observation strengthens the need for inclusion of a vertically applied load. It can be noted that in the range of F = 5-30 N, the values of the IT as well as its variation with the depth of penetration are quite insensitive to the value of the vertically applied load level. The increase in vertical load results in decrease of the IT during the "threads penetration" phase. This decrease is already visible for F = 60 N where the peak torque value at the wnd of the "treads penetration" is only 410 Nmm in comparison with 460 Nmm for the range of F = 5-30 N The IT start to decrease noticeably before F = 60 N, and for F = 90 N and beyond, its maximum values drop to below ~300 N*mm.

The IT of a trabecular bone with σ_Y = 10 MPa, for F = 5, 10, 20, 30, 40, 60, 80, 100 and 140 N, are shown in Fig. 11b. The range for which the IT values are less sensitive to the applied load is smaller than previously, in the range of F = 5-10 N. For higher values, F > 20 N, The IT decreases significantly. At F = 100 N the peak value at the end of the threads penetration is less than 130 Nmm. The bone loses its resisting torque at lower loads in comparison with a bone whose trabecular component has a strength of σ_Y = 62 MPa .

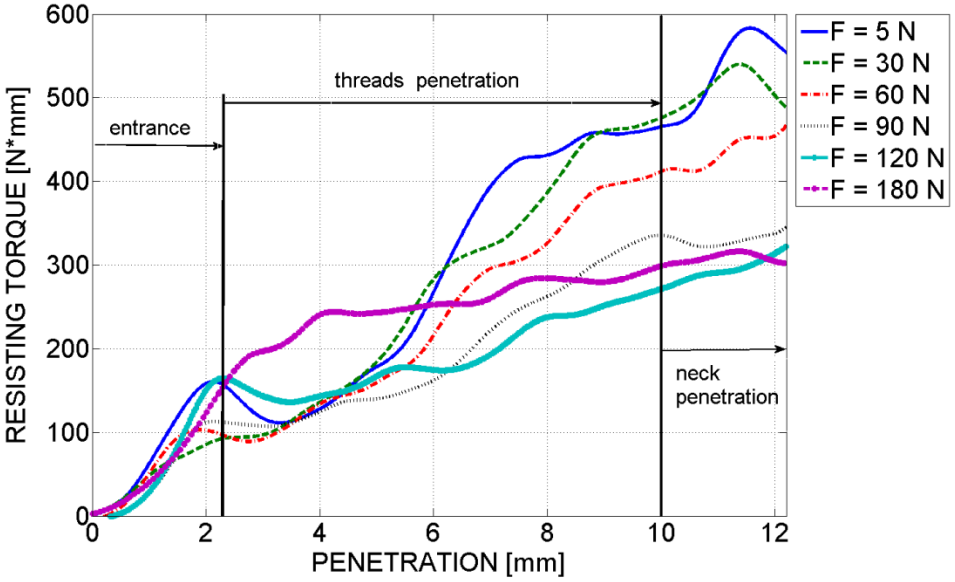

a.

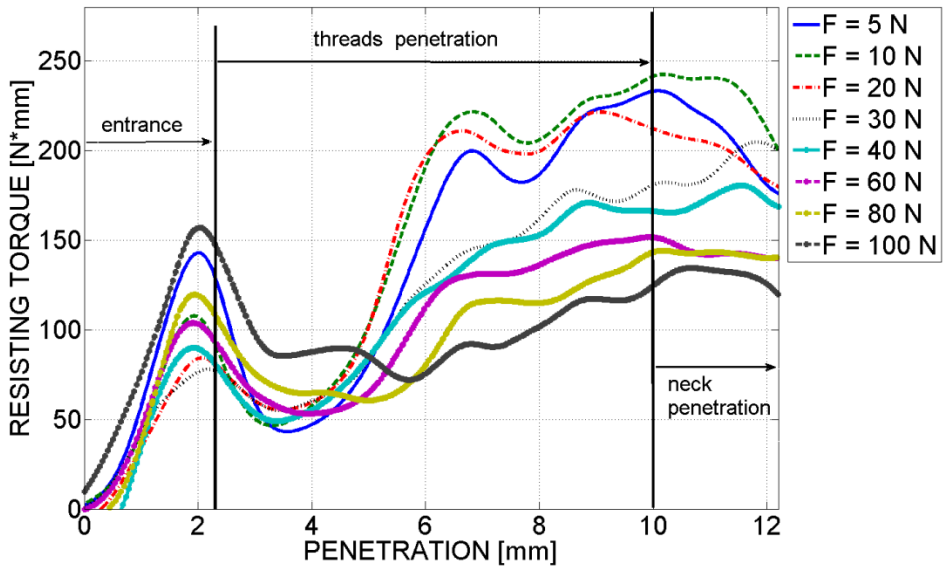

b.

Figure 11: a. The insertion torque for applied vertical forces F = 5, 10, 30, 60,90, 120, 150 and 180 N for trabecular bone having σ_Y = 62 MPa. b. The insertion torque for applied vertical forces F = 5, 10, 20, 30, 40, 60, and 100, N for a trabecular bone having σ_Y = 10 MPa.

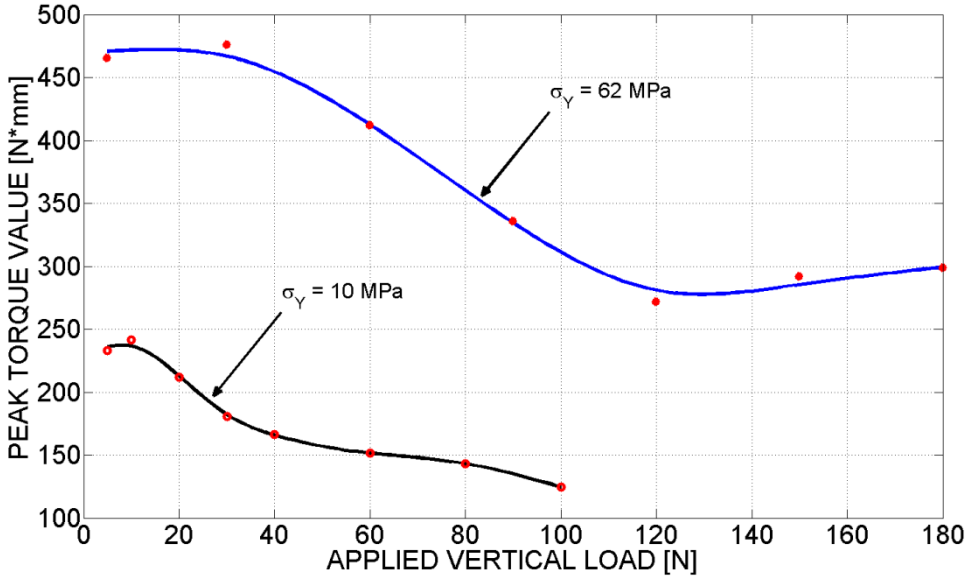

Figure 12: The peak torque values versus applied vertical load. The peak torques are measured at the end of the threads penetration for 10 mm depth of penetration.

Those results can be summarized by plotting the peak IT values at the end of the threads penetration (10 mm depth of penetration), for σ_Y = 62 MPa and σ_Y = 10 MPa, as shown in Fig. 12. The same kind of relation can be observed for the two strength levels, albeit with different values. Fig. 12 provides useful information for a "quick" estimation of the expected torque values as a function of the strength of the trabecular bone.

3.4.2 Effect on the number of implant revolution for full insertion

The relation between the applied vertical load and the number of revolutions of the implant for full insertion to depth of 13 mm is shown in Fig. 13 for σ_Y = 62 MPa and σ_Y = 10 MPa. Both curves indicate that with increasing load the number of revolutions decreases. *This means that in addition to the screwing insertion, the implant experiences additional extrusion.* For F = 5 N the number of revolutions is ~5.65 for both types of bones. The slope at F = 5 N indicates that for lower loads the number of revolutions increase. For F = 0 the number of revolution should increase to infinity. Up F =~ 80 N which correspond to ~4.55 revolutions for full insertion, both

curves behave similarly. This means that up to this load, the cortical bone is the component that mostly resists the applied load. For higher loads, the curve of the bone having σ_Y = 10 MPa drops rapidly due to the inability of the weak trabecular bone to resist the load, and the insertion process becomes mostly extrusion. For the bone having σ_Y = 62 MPa, the moderate reduction of the number of revolutions extends up to F =~150 N . For higher loads the insertion becomes again mostly extrusion.

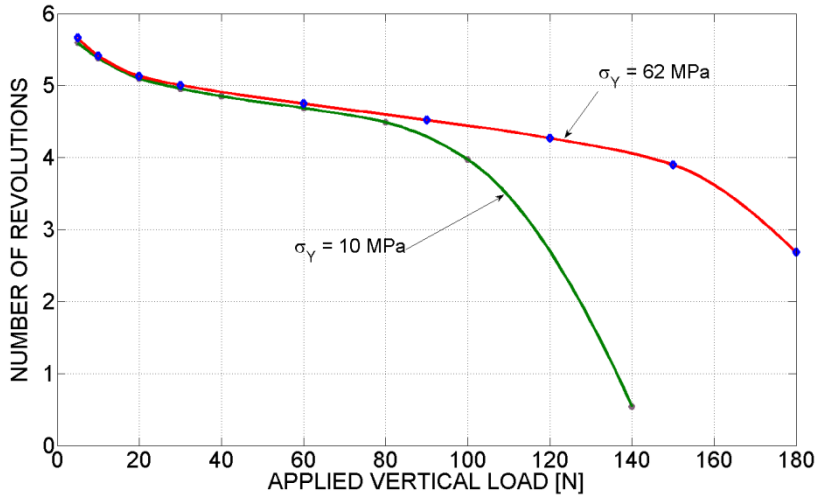

Figure 13: Effect of the vertical applied load on the number of implant revolutions for full insertion to depth of 13 mm.

3.4.3 Effect on bone damage

The damaged bone having σ_Y = 10 MPa and the deleted/failed elements at full insertion are shown in Fig. 14. The deformed bone, which was subjected to F=5 N, is shown in Figs 14a and the corresponding deleted undeformed elements are shown in Fig.14b. The deformed bone which was subjected to F=140 N is shown in Figs. 14c and the corresponding deleted undeformed elements are shown in Fig.14d . The curved threads in Fig. 14 a-b are easily distinguished and well outlined. By contrast, the threads in Fig.14c-d are destroyed due to extrusion.

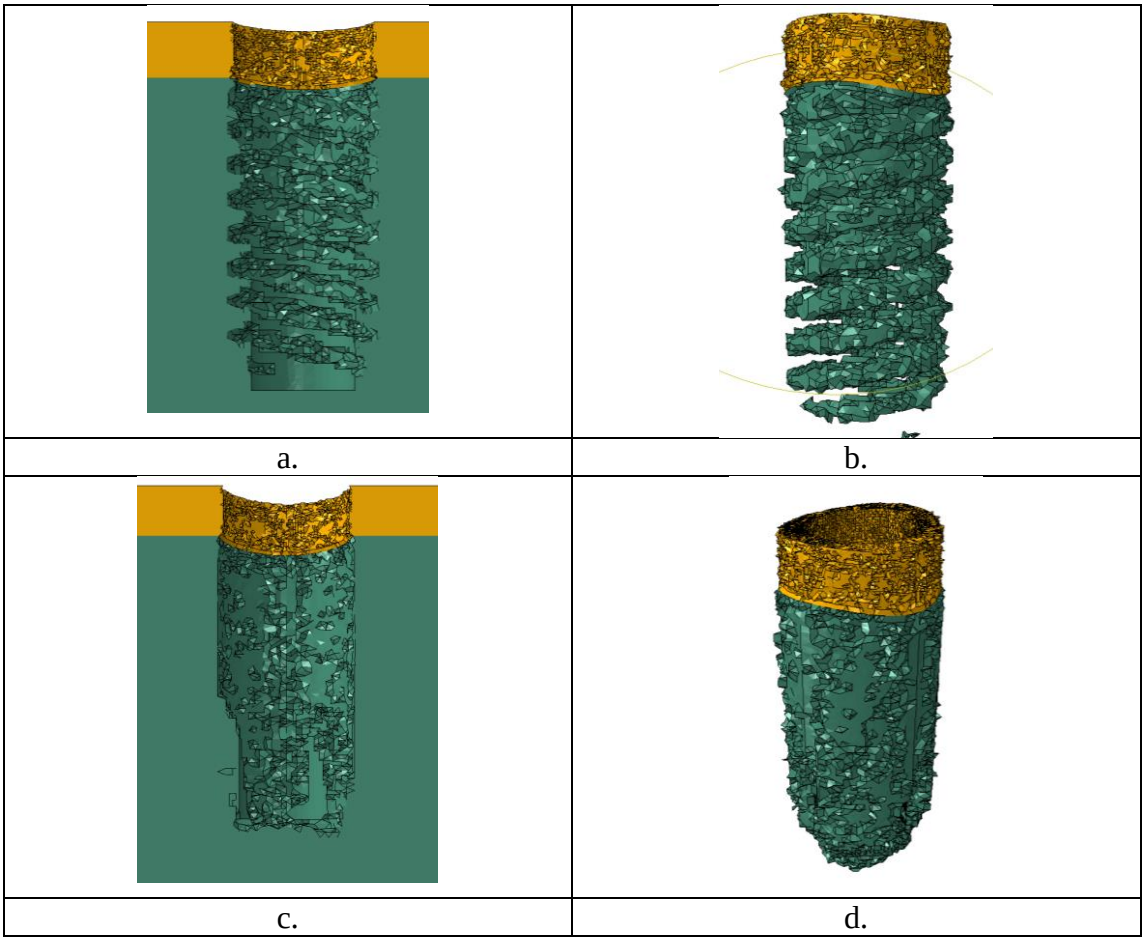

Figure 14: The damaged bone having σ_Y = 10 MPa and its deleted elements at full insertion for F = 5 N and F = 140 N. a. A cut view for F = 5 N. b. Isometric view of the undeformed deleted elements for F = 5 N. c. A cut view for F = 140 N. d. Isometric view of the undeformed deleted elements for F = 140 N.

4. Discussion

This research presents a thorough investigation of the implant insertion process, as experienced by the bone. The implant-bone interaction is deemed to affect the softer bone to a much more significant extent than it does affect the rigid implant.

This study examines two main issues. The first is the insertion torque, since the latter has been repeatedly identified as a predictor of the primary implant stability, which plays a significant role in the biological success of the implant. The second point of

interest concerns the bone itself, whether cortical or trabecular, and the state of damage that develops during the insertion process.

Several interesting results come out of the systematic finite element modeling that will be discussed in the following.

Nature of the torque

The first issue is the realization that torque is the *outcome* of the system characteristics, namely mechanical properties of the bone constituents, friction and possibly, the prescribed angular velocity. In other words, the torque is not prescribed but rather results from the problem at hand.

Need for a vertical load component

Another observation is that torque alone is not sufficient to insert a dental implant in the jawbone. In fact, a minimal vertical force should be (and is most likely) applied to the implant in order to initiate the insertion procedure. This force controls the amount of damage due to extrusion, since the insertion process comprises now *both screwing and extrusion*, noting that for low vertical loads, screwing dominates as opposed to extrusion at higher loads.

The present study identifies 2 limits for the vertical load component. The first is associated with the addition of an extrusion process to the dominant screwing process. This value is ~20 N for a trabecular bone having σ_Y = 10 MPa, and ~40 N for a trabecular bone having σ_Y = 62 MPa. The second limit is associated with the insertion becoming essentially an extrusion process. Here, value is ~80 N for a trabecular bone having σ_Y = 10 MPa. and ~150 N for a trabecular bone having σ_Y = 62 MPa. Beyond the second limit value, significant damage is inflicted to the trabecular bone resulting in the destruction of the thread due to extrusion, just like would occur in a normal threading process in which excessive normal pressure is applied (see Figs. 12 and 13). The additional extrusion process has implications on the primary stability of the implant since the insertion torque decreases significantly when excessive vertical load is applied.

Maximal and final torque values and torque evolution

Whereas the literature abounds in reports of final torque values, the present study and a few other experimental ones (O'Sullivan et al., 2000), provide a systematic characterization of the insertion torque evolution, as the implant traverses the cortical bone to start, then penetrates the trabecular bone, with the process ending by the penetration of the micro-grooves in the cortical bone. Let us note here that the micro-grooves of the selected specific implant geometry are not a general characteristic of all dental implants. However, when present, the microgrooves play a definite role during the last phase of the insertion process. They basically "erase" the thread of the cortical bone, thereby relieving the peri-implant stresses to a large extent.

Torque partition between the bone components

Another interesting outcome of the study is the partition of the insertion torque between the cortical and the trabecular bone. The first stage of cortical insertion is of course common to the two bone components. But an interesting observation is that the rest of the penetration process emphasizes the significant contribution of the trabecular bone to the insertion torque. For the specific implant geometry studied here, it was found that at the end of the last stage of insertion (neck penetration, the cortical bone looses its torque bearing capacity and the trabecular bone contribute solely to the torque. This observation complments to some extent that of Marquezan et al. (Marquezan et al., 2014) who concluded that the cancellous bone plays an important role in primary stability of mini-implants in the presence or absence of cortical bone. In other words, even if the latter is significantly weaker than the cortical bone, its frictional area is much larger than that of the cortical bone, thereby causing a significance insertion torque. Therefore, the mechanical strength of the trabecular bone is of prime relevance, and as mentioned earlier, this property is related to the bone density. The latter is well known to vary with age for instance [REF] (LEKHOLM, 1985)????, so that its variability is a factor to be accounted for.

Closure

This work shows the need to identify the bone quality for each individual to whom the implant is (will be) inserted. This parameter determines the whole evolution of the insertion torque value and its final value, which is considered to determine the implant's primary stability.

In other words, the present study clearly shows that if the implant geometry is well defined, and the bone geometry and properties are well known, or at least assessed by various methods, one can reasonably expect to *predict the insertion torque prior to the surgical procedure,* including a potential optimization stage in terms of implant geometry and applied load characteristics.

5. Conclusions

This work calculates the resisting torque during the insertion process of a dental implant into the mandible. This type of calculation is a *pre-operative* procedure as opposed to postoperative methods which are used today. The significance of this investigation is that the primary stability of an implant, which warranties to some extent its success, can now be modeled, predicted and tailored (optimized) on a personal basis, with the help of physically/clinically oriented numerical modeling. With the aid of such numerical analyses, one can predict and eventually maximize the chances of success of a dental implant, at least in terms of primary stability. In other words, numerical models of the kind presented here contribute to future Personalized Implant Dentistry.

References

Alsaadi, G., Quirynen, M., Michiels, K., Jacobs, R., Van Steenberghe, D., 2007. A biomechanical assessment of the relation between the oral implant stability at insertion and subjective bone quality assessment. J. Clin. Periodontol. 34, 359–366. doi:10.1111/j.1600-051X.2007.01047.x

Ashby, M.F., Medalist, R.F.M., 1983. The mechanical properties of cellular solids. Metall. Trans. A 14, 1755–1769. doi:10.1007/BF02645546

Atsumi, M., Park, S., Wang, H., 2007. Methods used to assess implant stability: current status. Oral Maxillofac. Implant.

Bardyn, T., G??det, P., Hallermann, W., B??chler, P., 2010. Prediction of dental implant torque with a fast and automatic finite element analysis: a pilot study. Oral Surgery, Oral Med. Oral Pathol. Oral Radiol. Endodontology 109, 594–603. doi:10.1016/j.tripleo.2009.11.010

Degidi, M., Piattelli, A., 2005. A 7-year Follow-up of 93 Immediately Loaded Titanium Dental Implants. J. Oral Implantol. 31, 25–31. doi:10.1563/0-730.1

Gibson, L.J., 1985. The mechanical behaviour of cancellous bone. J. Biomech. 18, 317–328. doi:10.1016/0021-9290(85)90287-8

Goswami, M.M., Kumar, M., Vats, A., Bansal, A.S., 2015. Evaluation of dental implant insertion torque using a manual ratchet. Med. J. Armed Forces India 71, S327–S332. doi:10.1016/j.mjafi.2013.07.010

Grant, J.A., Bishop, N.E., Götzen, N., Sprecher, C., Honl, M., Morlock, M.M., 2007. Artificial composite bone as a model of human trabecular bone: the implant-bone interface. J. Biomech. 40, 1158–64. doi:10.1016/j.jbiomech.2006.04.007

Guan, H., van Staden, R.C., Johnson, N.W., Loo, Y.-C., 2011. Dynamic modelling and simulation of dental implant insertion process—A finite element study. Finite Elem. Anal. Des. 47, 886–897. doi:10.1016/j.finel.2011.03.005

Hambli, R., 2013. Micro-CT finite element model and experimental validation of trabecular bone damage and fracture. Bone 56, 363–374. doi:10.1016/j.bone.2013.06.028

Hernandez, C.., Beaupré, G.., Keller, T.., Carter, D.., 2001. The influence of bone volume fraction and ash fraction on bone strength and modulus. Bone 29, 74–78. doi:10.1016/S8756-3282(01)00467-7

Javed, F., Ahmed, H.B., Crespi, R., Romanos, G.E., 2013. Role of primary stability for successful osseointegration of dental implants: Factors of influence and evaluation. Interv. Med. Appl. Sci. 5, 162–167. doi:10.1556/IMAS.5.2013.4.3

Javed, F., Romanos, G.E., 2010. The role of primary stability for successful immediate loading of dental implants. A literature review. J. Dent. 38, 612–620. doi:10.1016/j.jdent.2010.05.013

Kawahara, H., Kawahara, D., Hayakawa, M., 2003. Osseointegration under Immediate Loading: Biomechanical Stress–Strain and Bone Formation–Resorption. Implant.

Lee, J., Ozdoganlar, O.B., Rabin, Y., 2012. An experimental investigation on thermal exposure during bone drilling. Med. Eng. Phys. 34, 1510–1520. doi:10.1016/j.medengphy.2012.03.002

LEKHOLM, U., 1985. Patient selection and preparation. Tissue-integrated Prosthes. Osseointegration Clin. Dent. 199–209.

Marquezan, M., Lima, I., Lopes, R.T., Sant'Anna, E.F., Gomes De Souzac, M.M., 2014. Is trabecular bone related to primary stability of miniscrews? Angle Orthod. 84, 500–507. doi:10.2319/052513-39.1

Meredith, N., 2008. A Review of Implant Design, Geometry and Placement. Appl. Osseointegration Res. 6.

Meredith, N., Alleyne, D., Cawley, P., 1996. Quantitative determination of the stability of the implant-tissue interface using resonance frequency analysis. Clin. Oral Implants Res. 7, 261–267.

O'Sullivan, D., Sennerby, L., Meredith, N., 2000. Measurements comparing the initial stability of five designs of dental implants: a human cadaver study. Clin. Implant Dent. Relat. Res. 2, 85–92. doi:10.1111/j.1708-8208.2000.tb00110.x

Olsen, S., Ferguson, S.J., Sigrist, C., Fritz, W.-R., Nolte, L.P., Hallermann, W., Caversaccio, M., 2005. A novel computational method for real-time preoperative assessment of primary dental implant stability. Clin. Oral Implants Res. 16, 53–9. doi:10.1111/j.1600-0501.2004.01071.x

Orenstein, I.H., Tarnow, D.P., Morris, H.F., Ochi, S., 2000. Three-year post-placement survival of implants mobile at placement. Ann. Periodontol. 5, 32–41. doi:10.1902/annals.2000.5.1.32

Pandey, R.K., Panda, S.S., 2013. Drilling of bone: A comprehensive review. J. Clin. Orthop. Trauma 4, 15–30. doi:10.1016/j.jcot.2013.01.002

Pesqueira, A., Goiato, M., Filho, H., 2014. Use of stress analysis methods to evaluate the biomechanics of oral rehabilitation with implants. J. Oral.

Reilly, D.T., Burstein, A.H., 1974. The mechanical properties of cortical bone. J Bone Jt. Surg Am 56, 1001–1022.

Romanos, G., 2009. Bone quality and the immediate loading of implants—critical aspects based on literature, research, and clinical experience. Implant Dent.

Schulte, W., Lukas, D., 1992. The Periotest method. Int. Dent. J. 42, 433–40.

Schwartz-Dabney, C.L., Dechow, P.C., 2002. Edentulation Alters Material Properties of Cortical Bone in the Human Mandible. J. Dent. Res. 81, 613–617. doi:10.1177/154405910208100907

Simulia, 2014a. Abaqus/CAE version 6.14-2 (2014). Dassault Systèmes Simulia

Corp., Providence, RI, USA.

Simulia, 2014b. Abaqus/Explicit Version 6.14-2, Abaqus documentation . Dassault systemes, 2014.

Szmukler-Moncler, S., Piattelli, A., Favero, G. a, Dubruille, J.H., 2000. Considerations preliminary to the application of early and immediate loading protocols in dental implantology. Clin. Oral Implants Res. 11, 12–25. doi:10.1034/j.1600-0501.2000.011001012.x

Szmukler-Moncler, S., Salama, H., 1998. Timing of loading and effect of micromotion on bone-dental implant interface: review of experimental literature. J. Biomed.

TM, K., WC, H., 1992. Chapter 10: Mechanical properties of cortical and trabecular bone. Bone.

van Staden, R.C., Guan, H., Johnson, N.W., Loo, Y., Meredith, N., 2008. Step-wise analysis of the dental implant insertion process using the finite element technique. Clin. Oral Implants Res. 19, 303–13. doi:10.1111/j.1600-0501.2007.01427.x

Wang, W., Shi, Y., Yang, N., Yuan, X., 2014. Experimental analysis of drilling process in cortical bone. Med. Eng. Phys. 36, 261–6. doi:10.1016/j.medengphy.2013.08.006